NMR study of the ternary carbides M_2AlC (M=Ti,V,Cr)

C. S. Lue,* J. Y. Lin, and B. X. Xie
Department of Physics, National Cheng Kung University, Tainan 70101, Taiwan
(Received 8 September 2005; revised manuscript received 12 December 2005; published 26 January 2006)

We have performed a systematic study of the layered ternary carbides Ti_2AlC, V_2AlC, and Cr_2AlC using ^{27}Al NMR spectroscopy. The quadrupole splittings, Knight shifts, as well as spin-lattice relaxation times on each material have been identified. The sign of the isotropic Knight shift varies from positive for Ti_2AlC and V_2AlC to negative for Cr_2AlC, attributed to the enhancement of hybridization with increasing valence electron count in the transition metal. Universally long relaxation times are found for these alloys. Results provide a measure of Al-s Fermi-level density of states $N_s(E_F)$ for Ti_2AlC and V_2AlC. In addition, the evidence that $N_s(E_F)$ correlates with the transition metal d-electron count has been explored in the present NMR investigation.

DOI: 10.1103/PhysRevB.73.035125 PACS number(s): 71.20.Be, 76.60.−k

I. INTRODUCTION

Recently there has been a renewed interest in the ternary compounds of the form $M_{n+1}AX_n$ (where M is the early transition element, A is a group III A or IV A element, and X is C or N).[1] Among these phases, the materials with a general formula M_2AX, called the H or Hagg phase, exhibit a unique combination of properties such as high bulk modulus, high thermal and electrical conductivity, and good high-temperature oxidation resistance.[1,2] Although these carbides are ceramics, they demonstrate good damage tolerance and readily machinable.[1,3,4] Hence, a great deal of research has been devoted to investigating these materials for the understanding of their electronic properties and structural stability.[5–14]

For the present M_2AlC (M=Ti,V,Cr) carbides, they crystallized in the Cr_2AlC-type structure (the $P6_3/mmc$ space group) with the Wyckoff positions 4f for M, 2d for Al, and 2a for C, as shown in Fig. 1. Within this structure, the bonding between M and C is much stronger than that between M and Al, resulting in layered-like characteristics for the M-C planes. According to theoretically electronic structure calculations, carbon does not contribute significantly to the Fermi level density of states (DOS).[6,10] The Fermi surface features of these carbides are mainly characterized by hybridized M-d and Al-p states. Also the enhancement of the hybridization effect with increasing valence electron (VE) count in the transition atom has been proposed.[7–10] Nevertheless, there has been little experimental work associated with these scenarios, essential to interpret their electronic structures.

Nuclear magnetic resonance (NMR) is known as an atomic probe in metallic alloys yielding information on the bonding nature and Fermi surface features.[15,16] In this work, we will present NMR measurements including the Knight shifts, quadrupole transitions, as well as spin-lattice relaxation times in Ti_2AlC, V_2AlC, and Cr_2AlC as related to their local electronic characteristics. The information about the local environments is mainly obtained through the quadrupole interactions as well as through the hyperfine interactions in this investigation.

II. EXPERIMENT AND DISCUSSION

Polycrystalline compounds were prepared by an ordinary arc-melting technique. Briefly, a mixture of appropriate amounts of high-purity elemental metals was placed in a water-cooled copper hearth and then melted several times in an argon flow arc melter. Due to the volatility of Al at high temperatures, we started with excess Al for each sample, assuming that the weight loss during melting aroused entirely from the Al element. To promote homogeneity, these materials were annealed in a vacuum-sealed quartz tube at 900 °C for several days, and followed by furnace cooling.

Room-temperature x-ray diffraction taken with Cu $K\alpha$ radiation on powder specimens were consistent with the Cr_2AlC-type structure. Strong reflections in these alloys could be indexed according to the expected structure with several weak peaks remaining unidentified which had little effect on the NMR measurements. As one can see below, our NMR spectra clearly reveal that all studied carbides are well ordered, with one aluminum crystallographic site as expected. A more detailed analysis of the x-ray data, in which the $P6_3/mmc$ structure was refined with the Rietveld method. We thus obtained the lattice constants a=0.304 nm and c=1.360 nm for Ti_2AlC, a=0.291 nm and c=1.314 nm

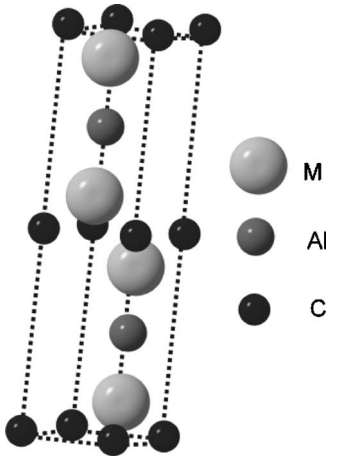

FIG. 1. Crystal structure for the Cr_2AlC-type carbides.

for V_2AlC, and $a=0.286$ nm and $c=1.282$ nm for Cr_2AlC. These values were found to be close to those reported in the literature.[17,18]

NMR measurements were performed using a Varian 300 spectrometer, with a constant field of 7.05 T. A home-built probe was employed for both room-temperature and low-temperature experiments.[19] Since the studied materials are metals, powder samples were used to avoid the skin depth problem of the rf transmission power. Each specimen was put in a plastic vial that showed no observable ^{27}Al NMR signal.[16] The Knight shifts here were referred to the ^{27}Al resonance frequency of one molar aqueous $AlCl_3$.

A. Quadrupole interaction and Knight shift

In this investigation, wide-line satellite spectra were mapped out by integrating spin echo signals of various excitations. For each studied carbide, there is a single Al site which is axially symmetric, leading to a symmetric one-site NMR spectrum, as demonstrated in Fig. 2. Due to electric quadrupole coupling, the ^{27}Al NMR spectrum $\left(I=\frac{5}{2}\right)$ is composed of five transition lines. For powdered samples, as in our experiment, these lines appear as typical powder patterns, with distinctive edge structures corresponding to the quadrupole parameters. The four edges are associated with $m=\pm\frac{1}{2}\leftrightarrow\pm\frac{3}{2}$ and $m=\pm\frac{3}{2}\leftrightarrow\pm\frac{5}{2}$ transitions. Since the first order quadrupole shift is the main effect shaping the satellite line, the quadrupole frequency, ν_Q, was determined directly from these lines. Results were tabulated in Table I. For V_2AlC, the high frequency side is strongly mixed with the ^{51}V NMR signals, and thus the corresponding ν_Q value was measured using the low-frequency satellite lines.

For the combination of electric quadrupole and axial Knight shift interactions, the shape and shift of the satellite lines can be expressed in the first order by

$$\nu(m\rightarrow m-1)=\nu_0\left\{1+\left[\frac{K_{ax}}{1+K_{iso}}+\frac{\nu_Q}{2\nu_o}\left(m-\frac{1}{2}\right)\right](3\cos^2\theta-1)\right\},\quad m\neq\frac{1}{2}. \tag{1}$$

Here ν_o is the pure Zeeman transition frequency in the absence of electric quadrupole and axial Knight shift interactions. K_{iso} and K_{ax} represent the isotropic Knight shift and axial Knight shift respectively, and θ is the angle between the crystal symmetry axis and the external magnetic field. The line shape simulation appropriate to the powder Ti_2AlC, V_2AlC, and Cr_2AlC samples were performed according to Eq. (1). The values of K_{ax} were obtained from the fit of central transition lines (below) because the second order quadrupole effect and the axial Knight shift interaction are of the same order of magnitude on the central transition splitting. Each synthetic profile which matches well with the experimental ^{27}Al NMR powder pattern, was plotted as a dotted curve in Fig. 2.

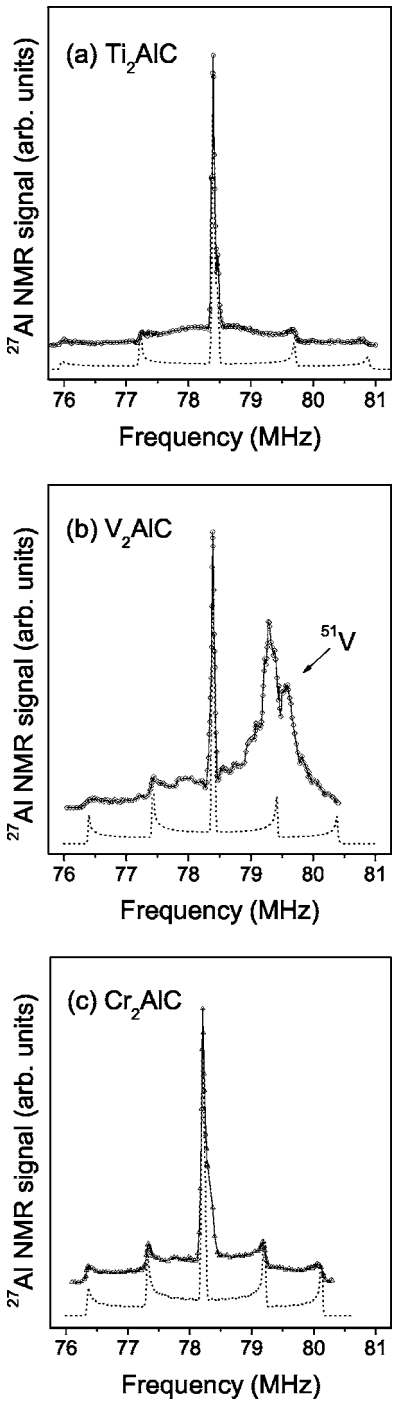

FIG. 2. Fully resolved satellite line shapes together with the best-synthetic curves for Ti_2AlC, V_2AlC, and Cr_2AlC. Each simulated curve has been shifted down for clarity.

From the ν_Q result, we can determine the electric field gradient (EFG) for each material. Here $\nu_Q=3eQV_{zz}/(2I-1)h$ is defined by the coupling between the nuclear quadrupole moment Q and the largest principal axis component of the EFG tensor V_{zz}. This effect arises from the noncubic arrangement of the charged lattice ions and the nonuniform charge density of the conduction electrons due to orbital motion. Attempts to reproduce the observed EFG's with a simple point-charge model yield unreasonable charge trans-

TABLE I. Quadrupole frequency, isotropic Knight shift, axial Knight shift, room-temperature spin-lattice relaxation time, and deduced Al-*s* Fermi level DOS (states/eV atom) for each studied alloy.

Alloy	ν_Q (MHz)	K_{iso} (%)	K_{ax} (%)	T_1 (ms)	$N_s(E_F)$
Ti_2AlC	2.48±0.05	0.074±0.002	0.020±0.005	140±20	0.014±0.001
V_2AlC	2.00±0.08	0.026±0.003	0.010±0.005	30±5	0.029±0.003
Cr_2AlC	1.90±0.03	−0.203±0.008	0.010±0.003	25±4	

fers. In fact, the electronegativity difference between transition metal and Al atoms is low and hence the bonding nature in the studied compounds cannot be entirely attributed to the ionicity. Alternatively, valence charges could be another source for the observed EFG's, pointing to the important Al-*M* hybridization in these compounds. Therefore the present ν_Q result suggests that both ionic and covalent mechanisms play significant roles for the bonding nature between *M* and Al atoms, being consistent with theoretical predications.[7–10]

Central transition $\left(m=\frac{1}{2}\leftrightarrow-\frac{1}{2}\right)$ line shapes for Ti_2AlC, V_2AlC, and Cr_2AlC, obtained from spin echo fast Fourier transforms using a standard $\pi/2-\tau-\pi$ sequence, were given in Fig. 3. Each spectrum is complicated by the simultaneous presence of anisotropic Knight shift and second-order quadrupole effects. For the present structure, the ^{27}Al quadrupole shift and the angle-dependent Knight shifts are axial. Hence the frequency shift for the central transition, $\Delta\nu$, to the second order quadrupole interaction and Knight shift can be written as[20]

$$\frac{\Delta\nu}{\nu_o}=\frac{K_{ax}}{1+K_{iso}}(3\cos^2\theta-1)+\frac{\nu_Q^2}{2\nu_o^2}(1-\cos^2\theta)(1-9\cos^2\theta). \tag{2}$$

For a polycrystalline sample, shape function fitting for the case of combined quadrupole and axial shift interactions was presented first by Jones *et al.*[21] By substituting the determined ν_Q and tuning K_{ax}, the positions of shoulders and singularities of each ^{27}Al NMR spectrum can be found. The best-simulated results yielded the corresponding room-temperature values for K_{iso} and K_{ax}, as summarized in Table I. The curve fits were evaluated by eye, and the values in Table I were used to produce the curve in Fig. 3. Note that in these fits the last digit quoted for K_{iso} and K_{ax} in the table make very little difference for the shape of the curves.

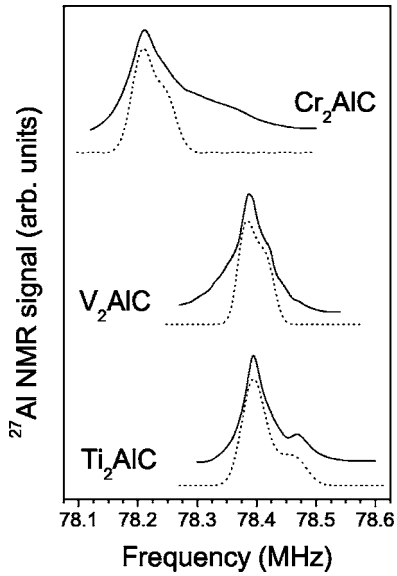

FIG. 3. ^{27}Al central transition NMR spectra for Ti_2AlC, V_2AlC, and Cr_2AlC measured at room temperature. The simulated curves, drawn as dotted lines, have been shifted for clarity.

The isotropic Knight shift here can be expressed as $K_{iso}=K_s+K_{orb}+K_{tr}$. The first term is associated with the *s*-contact Knight shift which is connected to the *s*-character Fermi-level DOS.[22] The second term is called the orbital Knight shift originating from the orbital electrons. The last one is due to the mixture of *d* states from transition metal element via transfer hyperfine interaction, which is related to the hybridization with *d* electrons. Although K_{orb} and K_{tr} are usually much smaller than K_s in paramagnetic metals, they become competitive when the *s*-character Fermi-level DOS is significantly small. This situation is suitable for the present carbides since the band structure calculations already indicated that the Al-*s* electrons contribute little to the Fermi-level DOS.[6,10] Indeed, this description is more obvious from the Cr_2AlC shift: negative ^{27}Al Knight shift for this material cannot be accounted for either by an ordinary *s*-contact term or by a paramagnetic orbital shift. On the other hand, the exchange polarization by *d* states generally contributes to a negative shift due to the negative hyperfine field of *d* electrons.[23–25] Accordingly, K_{tr} should be relatively small for Ti_2AlC, and the dominant K_s and K_{orb} terms produce a larger positive $K_{iso}=0.074\%$. For V_2AlC, K_{tr} is comparable with K_s+K_{orb}, resulting in a small positive $K_{iso}=0.026\%$. For Cr_2AlC, however, K_{tr} overcomes the contribution from K_s and K_{orb}, leading to a negative $K_{iso}=-0.203\%$. Hence the observed K_{iso} clearly reveals the enhancement of *p-d* hybridization with increasing the transition metal valence electron (VE) count. Such the analysis has been found to be consistent with those expected from the theoretical calculations, indicating that the *p-d* hybridization gradually increases with adding more transition metal valence electrons in M_2AlC.[7–10]

B. Spin-lattice relaxation time and Fermi level density of states

The spin-lattice relaxation time (T_1) measurements were carried out using the inversion recovery method. We recorded the signal strength by integrating the recovered spin echo signal. In these experiments, the relaxation process involves the adjacent pairs of spin levels, and the correspond-

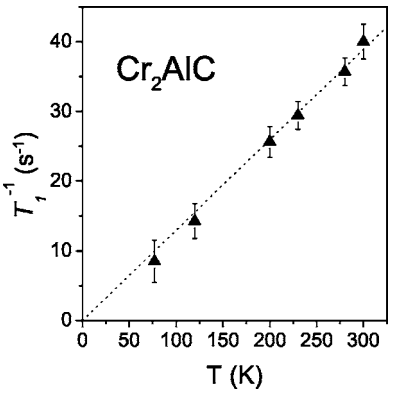

FIG. 4. Temperature-dependent ^{27}Al spin-lattice relaxation rate of Cr_2AlC. The Korringa behavior was indicated by the linear relationship, shown as a dotted line.

ing spin-lattice relaxation is a multiexponential expression.[26] For the central transition with $I=\frac{5}{2}$, the recovery of the nuclear magnetization follows:

$$\frac{M(t)-M(\infty)}{M(\infty)} = -2\alpha(0.257e^{-t/T_1}+0.267e^{-6t/T_1} + 0.476e^{-15t/T_1}). \quad (3)$$

Here $M(t)$ is the magnetization at the recovery time t and $M(\infty)$ is the magnetization after long time recovery. The parameter α is a fractional value derived from the initial conditions used in our experiments. Our T_1 values were thus obtained by fitting to this multiexponential recovery curve. To provide accurate values, each T_1 has been measured several times and the averaged T_1 for each material is enumerated in Table I. While nonconduction mechanisms may contribute to the relaxation, they were excluded by the Korringa relation.[27] T_1 measurements performed at various temperatures yield Korringa behavior (constant T_1T), indicating a conduction-electron mechanism for the observed relaxation.

It has been speculated that local magnetic moments may appear in Cr_2AlC. In further investigations, we examine the temperature dependence of the ^{27}Al central lines between room temperature and 77 K. The Knight shift exhibits nearly temperature independent, and the spin-lattice relaxation rate follows a Korringa relation, as demonstrated in Fig. 4. These observations indicate paramagnetic nature in Cr_2AlC. In fact, theoretical calculations for Cr_2AlC yielded marginal difference between antiferromagnetic (AFM) and paramagnetic configurations.[28] Also the determined local moment of $0.64\mu_B$ on the Cr site in the AFM phase will broaden the ^{27}Al NMR central transition line via magnetic dipolar interaction. This is contrary to the observed linewidth of about 40 KHz which is mainly splitted by the electric quadrupole effect.

The spin-lattice relaxation time measurement is known as a direct probe of the Fermi surface feature in nonmagnetic materials. For the present Ti_2AlC and V_2AlC alloys, the relaxation of Al nuclei is dominated by their coupling to the spin of the *s*-character electrons. For Cr_2AlC, however, its relative high transferred hyperfine field would make additional contribution to the relaxation rate. As a consequence, it is not quite appropriate to associate the observed T_1 with the Al-*s* Fermi-level DOS for the case of Cr_2AlC. In the absence of the collective electron effects, the relaxation rate is simply governed by the initial occupied and final unoccupied electronic states, associated with the hyperfine field arising from contact electrons. Under such the approximation, the spin-lattice relaxation rate can be written as[27]

$$\frac{1}{T_1} = 2hk_BT[\gamma_n H_{hf}^s N_s(E_F)]^2, \quad (4)$$

where h, k_B, and T are the Planck constant, Boltzmann constant, and absolute temperature, respectively. γ_n is the Al nuclear gyromagnetic ratio, H_{hf}^s is the hyperfine field per electron of the Al-*s* electrons at the Fermi level, and $N_s(E_F)$ represents the *s*-DOS at the Fermi level. As indicated from Table I, the deduced T_1's were found to be much longer than that of the Al metal which is about 6 ms at room temperature.[29] The strong enhancement of T_1 is related to DOS reduction at the Fermi level, consistent with the prediction given from theoretical calculations.

For Ti_2AlC and V_2AlC, the partial aluminum density of states around the Fermi surface are predominately *s* and *p* like, the mixture of *d* states being rather small. Since *p* and *d* hyperfine fields are generally an order of magnitude smaller than the *s*-character hyperfine field,[30] the main hyperfine field in such alloys arises from contact electrons. Taking $H_{hf}^s \sim 1.9\times10^6$ G in Al metal[30] and experimental T_1's, the Al-*s* Fermi level DOS of Ti_2AlC and V_2AlC can be obtained from Eq. (4), with the results listed in Table I.

From T_1 analysis, universally small $N_s(E_F)$ values are extracted for Ti_2AlC and V_2AlC, in good agreement with theoretical predications.[7,8,10] The deduced $N_s(E_F)$ value was found to increase with *d*-electron population as compared with both alloys. This tendency is consistent with the picture within a rigid-band scenario: the corresponding E_F shifts to higher DOS with increasing the transition metal VE count due to the band filling effect. Such an argument agrees well with the trend of the calculated total DOS of M_2AlC.[7–10] As a result, the higher DOS of V_2AlC compared to Ti_2AlC is reflected to its larger value of the bulk modulus.[1] Apparently the present NMR study would help to get an experimental understanding of the electronic band characteristics in these carbides.

III. CONCLUSIONS

We have a concise picture of the NMR features for Ti_2AlC, V_2AlC, as well as Cr_2AlC, giving experimental viewpoint for their local electronic properties. From the relaxation times, we extracted the Al-*s* Fermi-level DOS for Ti_2AlC and V_2AlC, which were found to correlate with the transition metal *d*-electron count. The Knight shift results provided an indication of the weight of *p*-*d* hybridization between Al-*p* and *M*-*d* electrons. We also have discussed the

observed EFG's, which reveal the important ionic and covalent bonding between Al and transition metal element in these carbides. Furthermore, a strong similarity was found for the NMR characteristics of these materials, pointing to a uniformity in their electronic structure properties.

ACKNOWLEDGMENTS

This work was supported by the National Science Council of Taiwan under Grant No. NSC-94-2112-M-006-001 (C.S.L).

*Electronic address: cslue@mail.ncku.edu.tw

[1] M. W. Barsoum, Prog. Solid State Chem. **28**, 201 (2000); and references therein.
[2] J. D. Hettinger, S. E. Lofland, P. Finkel, T. Meehan, J. Palma, K. Harrell, S. Gupta, A. Ganguly, T. El-Raghy, and M. W. Barsoum, Phys. Rev. B **72**, 115120 (2005).
[3] M. W. Barsoum and T. El-Raghy, J. Am. Chem. Soc. **79**, 1953 (1996).
[4] M. W. Barsoum, T. El-Raghy, C. J. Rawn, W. D. Porter, H. Wang, A. Payzant, and C. Hubbard, J. Phys. Chem. Solids **60**, 429 (1999).
[5] Y. Zhou and Z. Sun, Phys. Rev. B **61**, 12570 (2000).
[6] G. Hug and E. Fries, Phys. Rev. B **65**, 113104 (2002).
[7] Z. Sun, R. Ahuja, S. Li, and J. M. Schneider, Appl. Phys. Lett. **83**, 899 (2003).
[8] Z. Sun, R. Ahuja, and S. Li, Phys. Rev. B **68**, 224112 (2003).
[9] S. E. Lofland, J. D. Hettinger, K. Harrell, P. Finkel, S. Gupta, M. W. Barsoum, and G. Hug, Appl. Phys. Lett. **84**, 508 (2004).
[10] Z. Sun, D. Music, R. Ahuja, S. Li, and J. M. Schneider, Phys. Rev. B **70**, 092102 (2004).
[11] G. Hug, M. Jaouen, and M. W. Barsoum, Phys. Rev. B **71**, 024105 (2005).
[12] J. Wang, Y. Zhou, Z. Lin, F. Meng, and F. Li, Appl. Phys. Lett. **86**, 101902 (2005).
[13] R. Kumar, S. Rekhi, A. L. Cornelius, and M. W. Barsoum, Appl. Phys. Lett. **86**, 111904 (2005).
[14] J. M. Schneider, D. Music, Z. Sun, and R. Ahuja, J. Appl. Phys. **97**, 066105 (2005).
[15] C. S. Lue, S. Chepin, J. Chepin, and J. H. Ross, Jr., Phys. Rev. B **57**, 7010 (1998).
[16] C. S. Lue, B. X. Xie, S. N. Horng, and J. H. Su, Phys. Rev. B **71**, 195104 (2005).
[17] H. Nowotny, Prog. Solid State Chem. **2**, 27 (1970).
[18] J. C. Schuster, H. Nowotny, and C. Vaccaro, J. Solid State Chem. **32**, 213 (1980).
[19] C. S. Lue and B. X. Xie, Phys. Rev. B **72**, 052409 (2005).
[20] M. H. Cohen and F. Reif, *Solid State Physics* (Academic Press, New York, 1957), Vol. 5, p. 311.
[21] W. H. Jones, Jr., T. P. Graham, and R. G. Barnes, Phys. Rev. **132A**, 1898 (1969).
[22] C. P. Slichter, *Principles of Magnetic Resonance* (Springer-Verlag, New York, 1990).
[23] Y. Yafet and V. Jaccarino, Phys. Rev. **133**, A1630 (1964).
[24] *Metallic Shifts in NMR*, edited by G. C. Carter, L. H. Bennett, and D. J. Kahan (Pergamon, Oxford, 1977).
[25] C. S. Lue and J. H. Ross, Jr., Phys. Rev. B **60**, 8533 (1999).
[26] W. W. Simmons, W. J. O'Sullivan, and W. A. Robinson, Phys. Rev. **127**, 1168 (1962).
[27] J. Korringa, Physica (Amsterdam) **16**, 601 (1950).
[28] J. M. Schneider, Z. Sun, R. Mertens, F. Uestel, and R. Ahuja, Solid State Commun. **130**, 445 (2004).
[29] J. J. Spokas and C. P. Slichter, Phys. Rev. **113**, 1318 (1959); A. G. Anderson and A. C. Redfield, Phys. Rev. **116**, 583 (1959).
[30] G. C. Carter, I. D. Weisman, L. H. Bennett, and R. E. Watson, Phys. Rev. B **5**, 3621 (1972).